New Journal of Physics
The open access journal at the forefront of physics
Deutsche Physikalische Gesellschaft DPG IOP Institute of Physics

PAPER • OPEN ACCESS

Zero-bias anomaly and role of electronic correlations in a disordered metal film

To cite this article: Sangjun Jeon *et al* 2020 *New J. Phys.* **22** 083045

View the article online for updates and enhancements.

This content was downloaded from IP address 165.194.103.13 on 27/10/2020 at 08:08

IOP Publishing New J. Phys. 22 (2020) 083045 https://doi.org/10.1088/1367-2630/aba3e7

New Journal of Physics
The open access journal at the forefront of physics

Deutsche Physikalische Gesellschaft DPG
IOP Institute of Physics
Published in partnership with: Deutsche Physikalische Gesellschaft and the Institute of Physics

OPEN ACCESS

RECEIVED
1 April 2020

REVISED
22 June 2020

ACCEPTED FOR PUBLICATION
8 July 2020

PUBLISHED
17 August 2020

Original content from this work may be used under the terms of the Creative Commons Attribution 4.0 licence.

Any further distribution of this work must maintain attribution to the author(s) and the title of the work, journal citation and DOI.

PAPER

Zero-bias anomaly and role of electronic correlations in a disordered metal film

Sangjun Jeon[1], Sungmin Kim[2,3] and Young Kuk[4]

[1] Department of Physics, Chung-Ang University, Seoul 06974, Republic of Korea
[2] Physical Measurement Laboratory, National Institute of Standards and Technology, Gaithersburg, MD 20899, United States of America
[3] Institute for Research in Electronics and Applied Physics, University of Maryland, College Park, MD 20742, United States of America
[4] Daegu Gyeongbuk Institute of Science and Technology, Daegu 42988, Republic of Korea

E-mail: jsangjun@cau.ac.kr

Keywords: zero bias anomaly, dynamic Coulomb blockade, disorder, localization, electron correlation

Supplementary material for this article is available online

Abstract

Localization and electron correlation play significant roles in understanding the electronic states of low-dimensional systems. We carried out the tunneling spectroscopy measurements on a crystalline nano-sized island and a disordered two-dimensional metal film. The low temperature zero-bias anomaly was studied using $P(E)$ theory and statistical analysis of the spatial distribution of the local density of states in both the systems. The effective capacitance and resistance of the tunnel junction extracted from $P(E)$ theory gives the energy and temperature dependency of the measured ZBA. Statistical analysis reveals the electron correlation effect and the electron correlation length. By combining $P(E)$ theory and the statistical analysis, we found that the microscopic origin of ZBA formation in the disordered two-dimensional film is strongly related to the electron localization and the correlations.

1. Introduction

Localization theory, developed by Anderson *et al*, predicted the increase in resistivity of a disordered Fermi system at low temperatures due to the destructive interference of electron wave functions [1–4]. This unusual resistive behavior has been observed in various metallic and semiconducting systems [5, 6]. Following the initial prediction and observation, extensive experiments on disordered metallic systems led to the discovery of the zero-bias anomaly (ZBA) in conductance spectra [7–10]. A pioneering study by Altshuler and Aronov treated the electron–electron interaction perturbatively and reproduced the logarithmic temperature dependence of the resistivity and the ZBA in weak localization regimes [11, 12]. However, their model fails to describe the very low energy and low-temperature density of states (DOS) of disordered thin films [13]. It has been demonstrated using $P(E)$ theory that Coulomb interactions in a disordered system can be treated nonperturbatively by using the effective environmental parameters of tunnel junctions. This approach successfully describes not only the DOS character of the dynamic Coulomb blockade effect in ultra-small junctions but also the localization effect in disordered metallic systems and the low-temperature behavior of resistivity and low energy DOS [13, 14].

Low-temperature scanning tunneling microscopy (STM) studies on a sample with impurities showed significant suppression of the DOS at the Fermi level, owing to the electron–phonon interaction [15, 16], dynamic Coulomb blockade [17–19], and localization [20, 21]. Notably, the ZBA spectrum observed in ultra-small Pb islands and Pb wetting layers were well described by $P(E)$ theory, and the effective capacitance and resistance of the tunnel junction were extracted via fitting the measured data with the theory [17, 18]. However, the fitting parameters of $P(E)$ theory do not distinguish the various physical

© 2020 The Author(s). Published by IOP Publishing Ltd on behalf of the Institute of Physics and Deutsche Physikalische Gesellschaft

origins of the ZBA discussed above, and the many-body effects in disordered films cannot be understood fully from $P(E)$ theory.

In this article, we report STM and scanning tunneling spectroscopy (STS) studies on a disordered Pb film and crystalline Pb islands. The dI/dV spectrum acquired on both surfaces showed temperature-dependent ZBA, which were well described by $P(E)$ theory, as reported by other studies [17, 18]. To understand the physical origin of the ZBA, we studied the spatial correlation of the local density of states (LDOS) through the autocorrelation of the zero-energy DOS and the normalized DOS distribution from the STS data. The autocorrelation of the zero-energy DOS of the disordered Pb film follows exponential decay as a function of the distance, while that of the crystalline Pb island decays linearly. The DOS distribution of the disordered Pb film follows a log-normal distribution, while that of the crystalline Pb island follows Gauss-normal distribution. These statistical analyses of the disordered Pb film suggest that the microscopic origin of the ZBA developed on the disordered film is due to the electron localization and electronic correlations.

2. Results and discussion

The disordered Pb atomic film on top of Si (111) was prepared *in situ* in an ultra-high vacuum environment (base pressure $< 10^{-10}$ Torr), and STM and STS measurements were carried out with a home-built variable temperature STM. The tip and the sample are thermally connected to the cold stage, which is equipped with an internal heater. The measurement temperature of the tip and the sample was controlled simultaneously by a feedback controller (see supplementary materials section 2) (https://stacks.iop.org/NJP/22/083045/mmedia). Degenerately doped Si (111) with arsenic was used as a substrate, which was flash annealed at $T = 1250$ °C to form a Si (111)-(7 × 7) reconstructed surface. To control the substrate conduction, we prepared the silicon sample via ten cycles of annealing at 1250 °C for prolonged times (typically 60 s). The arsenic dopants diffuse easily inside silicon at this temperature and dissipate at the surface of silicon, which results in a reduced number of dopants near the surface [22]. The disordered 2D film was grown on top of this silicon substrate by thermally evaporating four monolayers (MLs) of Pb at room temperature. The extended high-temperature treatment depletes the dopants near the surface, and the formation of a disordered Pb film on top of silicon eliminates the dangling bonds of Si (111)-(7 × 7) and makes the silicon substrate effectively insulating at low temperatures. As a result, the Pb film formed on the silicon acts as a 2D conduction channel near the tunnel points. Figure 1(a) shows a typical STM topography of the prepared sample. Pb formed three MLs of a disordered wetting layer (colored blue in figure 1(a)), which covered the Si (111)-(7 × 7) surface, and the excessive Pb atoms formed the crystalline islands (colored yellow in figure 1(a)). Schematics of the sample configuration is shown in figure 1(b). The Pb island has a lateral area of 1626 nm^2 and a thickness of 2.0 nm, which corresponds to seven MLs of Pb films on top of a Pb wetting layer. The quantum well states developed on this island confirms the effective thickness and the crystal structure of the island [23] (see supplementary materials section 1).

Figures 1(c) and (d) display the spatially averaged STS measurements on the Pb island and the wetting layer, respectively. The blue curves are the averaged dI/dV spectra measured at 80 K, which show metallic DOS on the Pb island and broad suppression of the DOS on the wetting layer. The red curves in figures 1(c) and (d) are the averaged dI/dV spectra measured at 13 K. The low-temperature spectrum displays an unusual narrow dip at the Fermi level with a width of 17.5 mV on the island and an enhanced gap on the wetting layer. The normalized dI/dV intensity outside the gap feature is not affected by the measurement temperature. The measurement temperature was well above the superconducting critical temperature of the Pb island, which is typically 6 K for similar-sized Pb islands [24], and the size of the gap is one order of magnitude bigger than the superconducting gap (see supplementary materials section 2). We also checked that the temperature-independent quantum well states, and the resonance peaks are located at −550 mV and +610 mV on this island. Thus, the DOS suppression at low temperature is neither from the superconductivity nor from the quantized states.

We carried out position-dependent dI/dV measurements for both surfaces, the results of which are shown in figure 2. The topographic profile across the island edge shows a roughness of 1.7 Å for the Pb island and 4.3 Å for the wetting layer (figure 2(a)). The size and the density of the grain found in the Pb island are very similar to that of the clusters in the wetting layer. This similarity implies that the crystalline Pb island is formed after the disordered wetting layer, and the roughness of the underlying wetting layer is smoothened by the Pb island [17]. The ordered structure of the Pb island is further justified in figures 2(c) and (d), where we have plotted the individual dI/dV spectra measured for different spots on the Pb island (figure 2(c)) and the wetting layer (figure 2(d)). The dI/dV spectrum measured for the wetting layer show arbitrary LDOS in the high energy region ($|E| > 20$ mV) owing to the disorder and a reminiscence of Coulomb blockade. On the contrary, the dI/dV spectrum obtained for the island shows reasonably

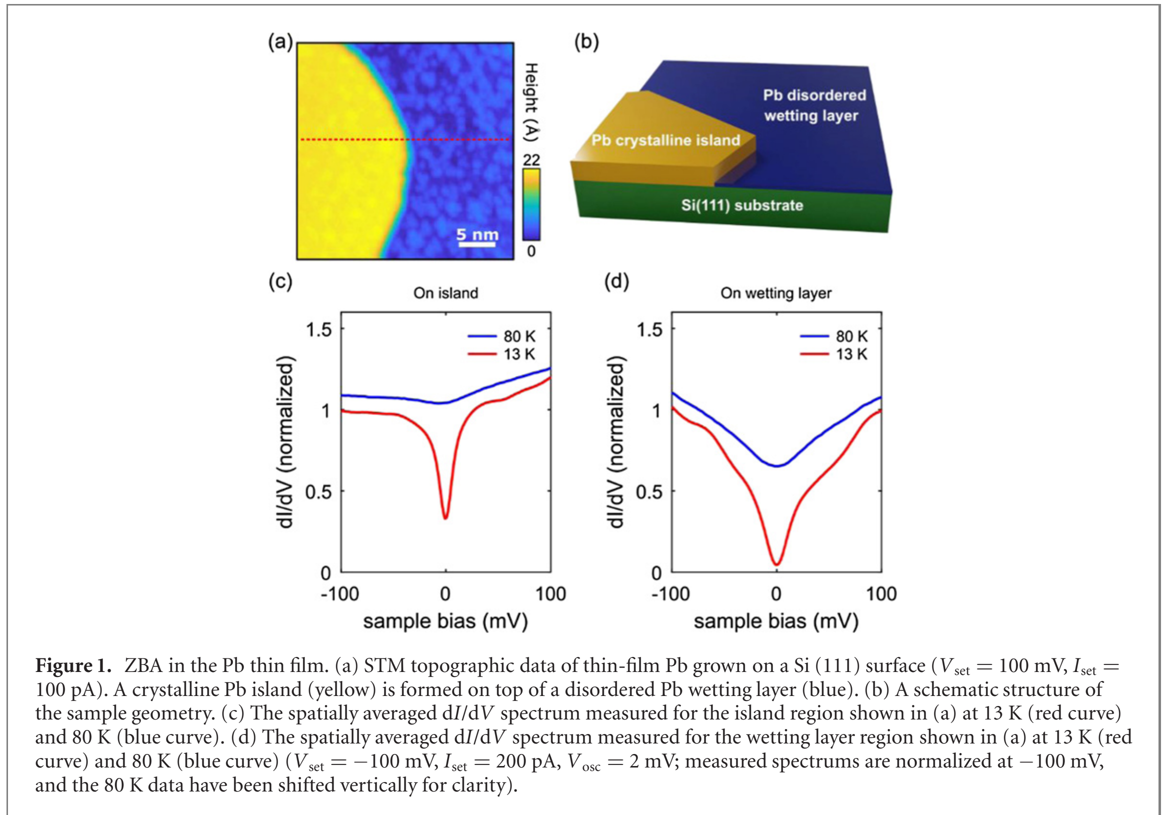

Figure 1. ZBA in the Pb thin film. (a) STM topographic data of thin-film Pb grown on a Si (111) surface ($V_{\mathrm{set}} = 100$ mV, $I_{\mathrm{set}} =$ 100 pA). A crystalline Pb island (yellow) is formed on top of a disordered Pb wetting layer (blue). (b) A schematic structure of the sample geometry. (c) The spatially averaged dI/dV spectrum measured for the island region shown in (a) at 13 K (red curve) and 80 K (blue curve). (d) The spatially averaged dI/dV spectrum measured for the wetting layer region shown in (a) at 13 K (red curve) and 80 K (blue curve) ($V_{\mathrm{set}} = -100$ mV, $I_{\mathrm{set}} = 200$ pA, $V_{\mathrm{osc}} = 2$ mV; measured spectrums are normalized at −100 mV, and the 80 K data have been shifted vertically for clarity).

homogeneous LDOS over the broad energy window, which is a consequence of the ordered atomic structure of the island. Interestingly, the DOS suppressions around the Fermi level for both surfaces are surprisingly well overlapped to other DOS measured on the same surface, and the variation of the normalized zero-bias conductance is suppressed for both surfaces, as shown in figure 2(b). This relatively homogeneous dI/dV spectrum at low energy indicates the STS measurements with the STM set bias ($V_{\mathrm{set}} =$ −100 mV) adequately reflect the absolute LDOS. The temperature-dependent dI/dV spectrum shown in figure 1 and the energetically symmetric shape of the gap around the Fermi level shown in figure 2 strongly suggest that the origin of the dip in the DOS is related to the symmetrical energy loss in the dynamical Coulomb blockade of the ultra-small tunnel junctions.

$P\,(E)$ theory successfully described the ZBA observed in ultra-small tunnel junctions and disordered metallic systems [17–19, 21]. Instead of using the conventional elastic tunnel assumption, the $P\,(E)$ function incorporates the energy-dependent capacitive noise effect as well as the interaction effects in a disordered system in the tunneling process [25]. The modified tunneling probability is

$$\vec{\Gamma}\,(V) = \frac{1}{e^2 R_{\mathrm{T}}}\int_{-\infty}^{\infty}\int_{-\infty}^{\infty} \mathrm{d}E\,\mathrm{d}E' n_{\mathrm{t}}\,(E)\,n_{\mathrm{s}}\left(E' + eV\right) f\,(E)\left[1 - f\left(E' + eV\right)\right] P\left(E - E'\right),$$

where n_{t} and n_{s} are the DOS of the tip and the sample, respectively, $f\,(E)$ is the Fermi–Dirac distribution, and R_{T} is the tunneling resistance. $P\,(E)$ is generally defined as

$$P\,(E) = \frac{1}{2\pi\hbar}\int_{-\infty}^{\infty} \mathrm{d}t\ \exp\left[J\,(t) + \frac{i}{\hbar}Et\right].$$

$J\,(t)$ is the phase—phase correlation function, which has the form

$$J\,(t) = 2\int_0^{\infty} \frac{\mathrm{d}\omega}{\omega}\frac{\mathrm{Re}Z\,(\omega)}{R_{\mathrm{K}}}\frac{\mathrm{e}^{-\mathrm{i}\omega t} - 1}{1 - \mathrm{e}^{-\hbar\omega/k_{\mathrm{B}}T}},$$

where T is the temperature, and $R_{\mathrm{K}} = h/e^2$. The total impedance $Z(\omega)$ of the STM tunnel junction is defined as

$$Z\,(\omega) = \frac{1}{\mathrm{i}\omega C_J + 1/R_{\mathrm{env}}}.$$

We used numerical methods described in [19] to calculate $J(t)$ and $P(E)$ and extracted the resistance (R_{env}) and junction capacitance (C_J) of the environmental impedance by fitting the measured STS data. The effective circuit diagram of the tunnel junction is shown in the inset of figure 3(c).

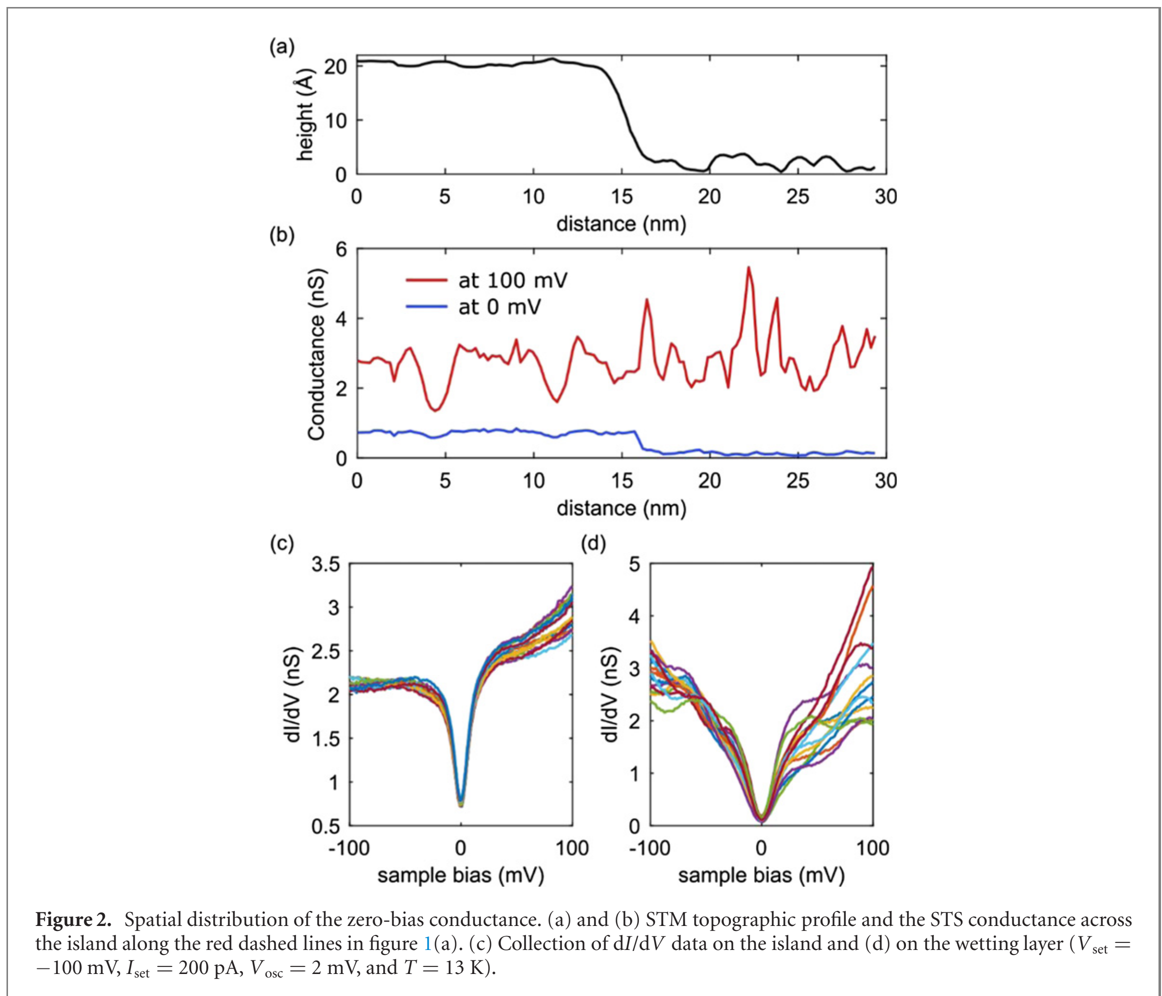

Figure 2. Spatial distribution of the zero-bias conductance. (a) and (b) STM topographic profile and the STS conductance across the island along the red dashed lines in figure 1(a). (c) Collection of dI/dV data on the island and (d) on the wetting layer ($V_{\mathrm{set}} = -100$ mV, $I_{\mathrm{set}} = 200$ pA, $V_{\mathrm{osc}} = 2$ mV, and $T = 13$ K).

The STS data obtained along with the red dashed line in figure 1(a) is displayed in a color plot (figure 3(a)). The edge of the Pb island is located at 13 nm in this plot. As we have seen in figures 2(c) and (d), the DOS suppression at zero energy shown in figure 3(a) is very uniform over the long lateral distance and does not vary with the local DOS variation related to the disorder in the Pb film. Figure 3(b) is the averaged dI/dV data obtained for the island region (blue dots) and the wetting layer region (yellow dots). The solid line in figure 3(b) is the fitted curve from $P(E)$ theory. We used the energy window from -15 mV to 15 mV for the STS data (gray region in figure 3(b)) to extract the environmental parameters that are not altered by the DOS variation (the fitting method is described in supplementary materials section 4). The dashed lines in figure 3(b) are the dI/dV data simulated using the same fitting parameters at 80 K. The temperature dependency of the STS data shown in figures 1(c) and (d) is well captured by $P(E)$ theory. The spatial distribution of the environmental parameters are plotted in figure 3(c) which shows a homogeneous environmental resistance ($R_{\mathrm{env}} = 6.64 \pm 0.03\,\mathrm{k}\Omega$) over the whole measurement range, whereas the average junction capacitance of the wetting layer ($\overline{C_J} = 2.90 \pm 0.21$ aF) is smaller than that of the Pb island ($\overline{C_J} = 8.83 \pm 0.11$ aF). The homogeneous environmental resistance of both the wetting layer and island suggests that the sample resistance is mainly limited by the electrical behavior of the wetting layer [18]. The extracted junction capacitance and resistance of the Pb island are comparable to those from previous reports, where nano-sized islands were grown on top of an insulating film [18]. However, the capacitance of the wetting layer is significantly smaller than that of a wetting layer from a similar study [17]. It can be related to the doping dependent conductivity and the dielectric constant of the silicon substrate.

In general, the resistance of the sample R compared to the resistance quantum $R_{\mathrm{K}} = h/e^2 = 25.8\,\mathrm{k}\Omega$ defines the regime of the electron behavior in the sample. The system is in the diffusive regime when $R/R_{\mathrm{K}} \ll 1$ and in the strong localization regime when $R/R_{\mathrm{K}} \gg 1$. In this study, since the calculated resistance of the sample is comparable to the resistance quantum ($R_{\mathrm{env}}/R_{\mathrm{K}} =\sim 1$), we can regard the system as being in the intermediate regime, where the LDOS develops ZBA at the Fermi level. Moreover, we found that the dI/dV spectra obtained at the wetting layer exhibited bumps that are symmetrically located around the Fermi energy, as shown in figure 2(d). These features can be understood as a reminiscence of the Coulomb blockade that develops conductance enhancement at the Coulomb energy of the system, defined

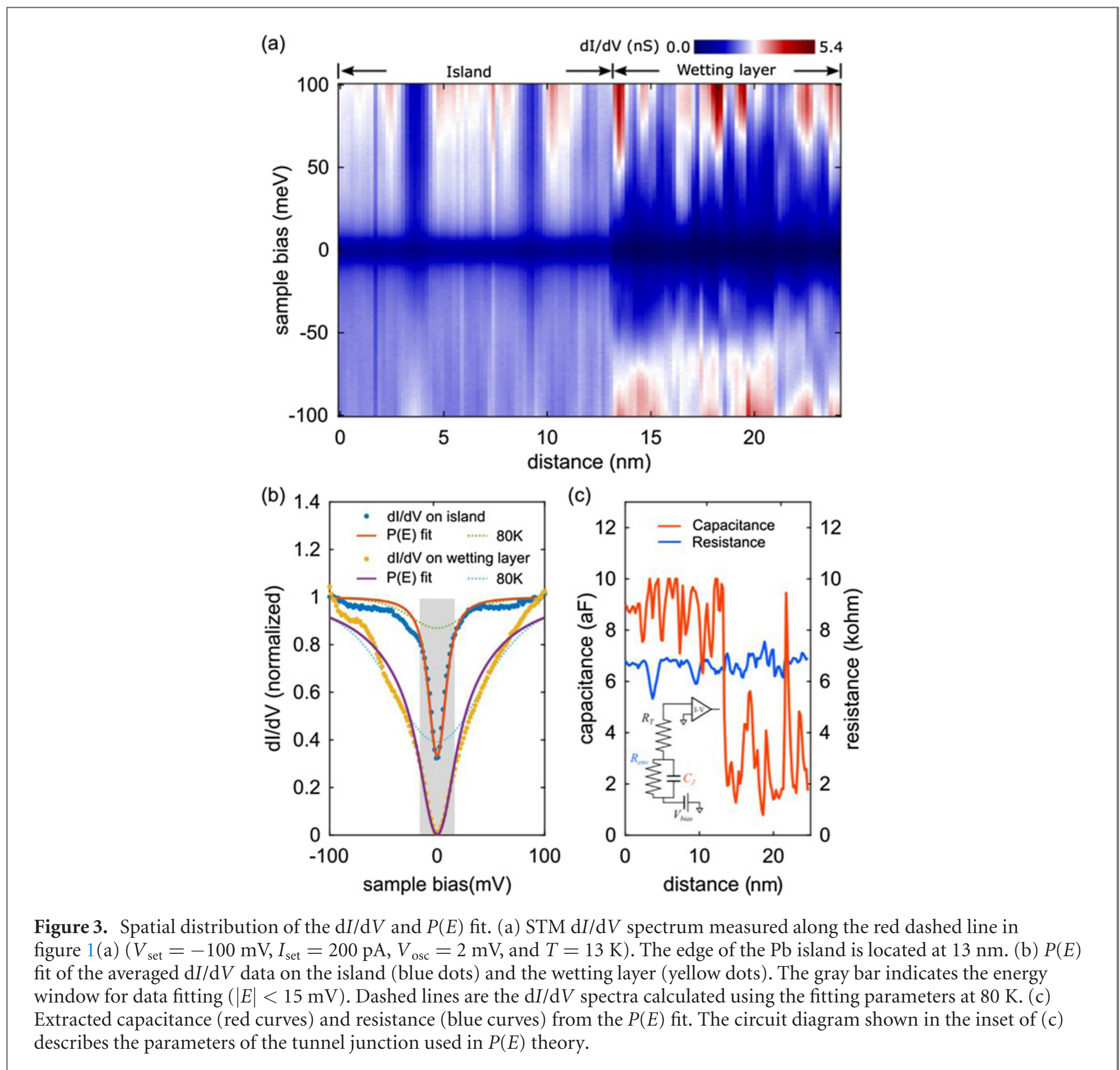

Figure 3. Spatial distribution of the dI/dV and $P(E)$ fit. (a) STM dI/dV spectrum measured along the red dashed line in figure 1(a) ($V_{set} = -100$ mV, $I_{set} = 200$ pA, $V_{osc} = 2$ mV, and $T = 13$ K). The edge of the Pb island is located at 13 nm. (b) $P(E)$ fit of the averaged dI/dV data on the island (blue dots) and the wetting layer (yellow dots). The gray bar indicates the energy window for data fitting ($|E| < 15$ mV). Dashed lines are the dI/dV spectra calculated using the fitting parameters at 80 K. (c) Extracted capacitance (red curves) and resistance (blue curves) from the $P(E)$ fit. The circuit diagram shown in the inset of (c) describes the parameters of the tunnel junction used in $P(E)$ theory.

by the effective capacitance of the system [26]. The broadening shown in the individual dI/dV spectrum is related to the incomplete isolation of the sample, owing to the leakage path through the wetting layer. If we regard the shoulder of the dI/dV spectrum as the onset of the Coulomb blockade gap, the size of the first gap is approximately 50 mV, and the second gap is approximately 150 mV, which corresponds to capacitance values of 3.2 aF and 1.0 aF, respectively. These values are close to the derived capacitance of the wetting layer from $P(E)$ theory and the tip-sample capacitance (see further details in supplementary materials section 3).

To understand the electron localization effect in this system, we calculated the normalized autocorrelation Corr (E, r) from the spatially resolved tunneling conductance $G(E, r)$ along the straight line over the wetting layer.

$$\mathrm{Corr}\,(E, r) = \int \mathrm{d}r' \mathrm{G}\left(E, r'\right) \times G\left(E, r' + r\right) / \mathrm{Corr}_0(E)$$

where $\mathrm{Corr}_0\,(E) = \int \mathrm{d}r' \mathrm{G}\left(E, r'\right)^2$. The contour plots of the autocorrelation Corr (E, r) obtained for the island and the wetting layer are plotted in figures 4(a) and (b). Each curve represents the lateral position of the constant autocorrelation strength as a function of sample bias. As can be seen in figure 4(a), the autocorrelation decays linearly in the space on the island for all sample biases measured in this study. The autocorrelation decreases with distance on the wetting layer as well, but the decay rate highly depends on the sample bias. Notably, the autocorrelation near the zero energy decays fast at a short distance ($r < 4$ nm) and decays slowly at further distances. Figure 4(c) displays the energy-dependent autocorrelation of LDOS obtained at 0 mV and 70 mV, which emphasizes the spatial variations of the autocorrelation. The autocorrelation of LDOS collected on the Pb island (blue square and black cross in figure 4(c)) decays slower than the one obtained for the wetting layer (green triangle and red diamond in figure 4(c)). Moreover, the autocorrelation of zero-energy LDOS obtained for the wetting layer decays nonlinearly (red

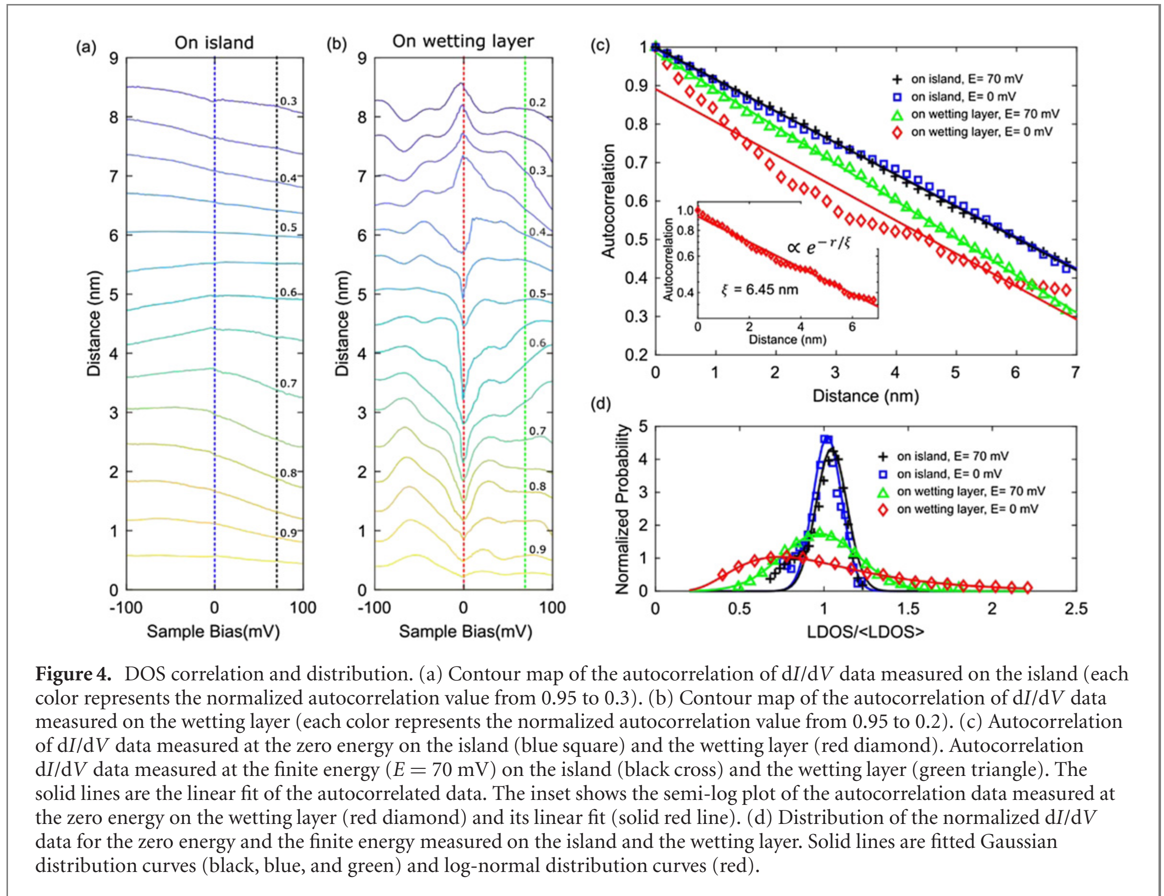

Figure 4. DOS correlation and distribution. (a) Contour map of the autocorrelation of $\mathrm{d}I/\mathrm{d}V$ data measured on the island (each color represents the normalized autocorrelation value from 0.95 to 0.3). (b) Contour map of the autocorrelation of $\mathrm{d}I/\mathrm{d}V$ data measured on the wetting layer (each color represents the normalized autocorrelation value from 0.95 to 0.2). (c) Autocorrelation of $\mathrm{d}I/\mathrm{d}V$ data measured at the zero energy on the island (blue square) and the wetting layer (red diamond). Autocorrelation $\mathrm{d}I/\mathrm{d}V$ data measured at the finite energy ($E = 70$ mV) on the island (black cross) and the wetting layer (green triangle). The solid lines are the linear fit of the autocorrelated data. The inset shows the semi-log plot of the autocorrelation data measured at the zero energy on the wetting layer (red diamond) and its linear fit (solid red line). (d) Distribution of the normalized $\mathrm{d}I/\mathrm{d}V$ data for the zero energy and the finite energy measured on the island and the wetting layer. Solid lines are fitted Gaussian distribution curves (black, blue, and green) and log-normal distribution curves (red).

diamond), and it decays exponentially according to Corr $(r) \propto \mathrm{e}^{-r/\xi}$ and $\xi = 6.45$ nm, as shown in the inset of figure 4(c).

The localization length $\xi = \ell \exp(\pi k_F \ell)$ (where ℓ is the mean free path) and the thermal diffusion length $L_\mathrm{T} = \sqrt{\hbar D/k_\mathrm{B}T}$ (where D is the diffusion coefficient, and the T is the temperature) governs the low temperature electronic behaviors of the system in the strong localization regime and in the diffusive regime, respectively. The localization length depends on the electron conductivity as the formula indicates, and the thermal diffusion length increases with decreasing temperature. Thus, the crossover from the diffusive regime to the strong localization regime occurs at the temperature where $R/R_\mathrm{K} =\sim 1$. Considering the high resistivity of the sample in this study, the estimated thermal diffusion length L_T is about 11 nm with the diffusion coefficient $D = 2\,\mathrm{cm}^2\,\mathrm{s}^{-1}$. This long thermal diffusion length at 13 K compared to the decay length ξ extracted from the decay rate of the autocorrelation suggests that the measurement temperature is below the crossover temperature and the electron localization mainly dominates the electronic properties of the sample.

The LDOS distribution shows the electron interaction effect in the disordered system. The noninteracting electron system is predicted to have a Gaussian normal distribution, since the LDOS is randomly distributed without correlation, while the interacting electron system follows the log-normal distribution [4, 21]. Figure 4(d) displays the distribution of LDOS along a straight line of 10 nm length on the island and the wetting layer, respectively. The x-axis represents the LDOS normalized by the mean value $\langle\mathrm{LDOS}\rangle$, and the y-axis is the probability of finding the normalized LDOS value. As seen in figure 4(d), the LDOS obtained for the island follows the Gaussian normal distribution with the mode at 1.04 ($E = 70$ mV, black curve in figure 4(d)) and 1.02 ($E = 0$ mV, blue curve in figure 4(d)) from the fitting. Although the LDOS distribution measured on the wetting layer with energy 70 mV shows a standard deviation of 0.23, which is three times broader than the LDOS distribution determined for the island, the LDOS distribution fits into the Gaussian-normal distribution with the mode at 0.98. On the contrary, the LDOS distribution measured for the wetting layer with energy 0 mV shows a skewed distribution that was not symmetric about the mode that is located at 0.75. This skewed LDOS distribution follows log-normal distribution when the length of the measured STS is longer than the decay length ξ. This unusual LDOS distribution strongly suggests that the electron correlation plays a crucial role in developing ZBA on the disordered surface. In contrast, the origin of the ZBA developed on the Pb island is not likely due to the electron correlation.

3. Conclusion

We examined a crystalline Pb island and a disordered Pb wetting layer with a high spatial and energy resolution. We observed temperature dependent ZBA on both the ordered and disordered surfaces at low temperatures. $P(E)$ theory confirmed the overall ZBA features. However, the calculated environmental parameters did not distinguish the microscopic origin of the ZBA that appeared on both surfaces. By analyzing the spatial statistics of the STS, we found that the autocorrelation of the zero-energy STS acquired along the wetting layer decayed exponentially with the decay length $\xi = 6.45$ nm, and the distribution of the STS followed a log-normal distribution. Thus, the many-body effect, along with the electron localization, needs to be considered simultaneously to understand the physical origin of ZBA developed in the wetting layer. In contrast, the ZBA formed on the island can be understood from a single-electron picture with a Coulomb interaction.

The Anderson localization due to a disorder and the many-body effect due to electron correlations are the main factors that can change a metal into an insulating phase [27]. By analyzing the spatially resolved electronic states and their statistics, we proved that the electronic behavior of the Pb wetting layer originated from both the electron localization and electron correlations. This new finding can be generalized to a low dimensional system to understand the role of electronic correlation effects and to obtain the electron correlation length. Moreover, systematic studies on the Pb wetting layer under various environmental conditions can demonstrate the microscopic mechanism of metal–insulator transition in disordered metal films.

Conflict of interest

There are no conflicts to declare.

Acknowledgments

This research was supported by the National Research Foundation of Korea (NRF) grant funded by the Korea government (MSIT) (No. NRF-2019R1F1A1060058) and supported by the Chung-Ang University Research Grants in 2018.

ORCID iDs

Sangjun Jeon https://orcid.org/0000-0002-3134-7838

References

[1] Abrahams E, Anderson P W, Licciardello D C and Ramakrishnan T V 1979 *Phys. Rev. Lett.* **42** 673
[2] Anderson P W, Abrahams E and Ramakrishnan T V 1979 *Phys. Rev. Lett.* **43** 718
[3] Anderson P W 1958 *Phys. Rev.* **109** 1492
[4] Lee P A and Ramakrishnan T V 1985 *Rev. Mod. Phys.* **57** 287
[5] Dolan G J and Osheroff D D 1979 *Phys. Rev. Lett.* **43** 721
[6] Bishop D J, Tsui D C and Dynes R C 1980 *Phys. Rev. Lett.* **44** 1153
[7] Davydov D N, Mayou D, Berger C, Gignoux C, Neumann A, Jansen A G M and Wyder P 1996 *Phys. Rev. Lett.* **77** 3173
[8] Klein T, Symko O G, Davydov D N and Jansen A G M 1995 *Phys. Rev. Lett.* **74** 3656
[9] Zeller H R and Giaever I 1969 *Phys. Rev.* **181** 789
[10] Escudero R, Lasjaunias J C, Calvayrac Y and Boudard M 1999 *J. Phys.: Condens. Matter.* **11** 383
[11] Altshuler B L and Aronov A G 1979 *Solid State Commun.* **30** 115
[12] Altshuler B, Aronov A and Lee P A 1980 *Phys. Rev. Lett.* **44** 1288
[13] Ingold G L and Grabert H 1991 *EPL* **14** 371
[14] Rollbühler J and Grabert H 2001 *Phys. Rev. Lett.* **87** 126804
[15] Matsuda I *et al* 2007 *Phys. Rev. Lett.* **99** 146805
[16] Wang K, Zhang X, Loy M M T, Chiang T-C and Xiao X 2009 *Phys. Rev. Lett.* **102** 076801
[17] Serrier-Garcia L, Cuevas J C, Cren T, Brun C, Cherkez V, Debontridder F, Fokin D, Bergeret F S and Roditchev D 2013 *Phys. Rev. Lett.* **110** 157003
[18] Brun C, Müller K H, Hong I-P, Patthey F, Flindt C and Schneider W-D 2012 *Phys. Rev. Lett.* **108** 126802
[19] Ast C R, Jäck B, Senkpiel J, Eltschka M, Etzkorn M, Ankerhold J and Kern K 2016 *Nat. Commun.* **7** 13009
[20] Hirahara T, Komorida T, Gu Y, Nakamura F, Idzuchi H, Morikawa H and Hasegawa S 2009 *Phys. Rev.* B **80** 235419
[21] Richardella A, Roushan P, Mack S, Zhou B, Huse D A, Awschalom D D and Yazdani A 2010 *Science* **327** 665
[22] Wang K, Zhang X, Loy M and Xiao X 2008 *Surf. Sci.* **602** 1217
[23] Wei C M and Chou M Y 2002 *Phys. Rev.* B **66** 233408

[24] Kim J, Fiete G, Nam H, Macdonald A and Shih C 2011 *Phys. Rev.* B **84** 14517
[25] Ingold G-L and Nazarov Y V 1992 *Single Charg. Tunneling. NATO ASI Ser.* (Series B Physics) (Berlin: Springer) pp 21–107
[26] Hong I-P, Brun C, Pivetta M, Patthey F and Schneider W-D 2013 *Front. Physiol.* **1** 1
[27] Imada M, Fujimori A and Tokura Y 1998 *Rev. Mod. Phys.* **70** 1039